Journal of Fluids and Structures (1997) **11,** 465–484

SEMI-ANALYTICAL FORMULATION FOR SECOND-ORDER DIFFRACTION BY A VERTICAL CYLINDER IN BICHROMATIC WAVES

R. Eatock Taylor and J. B. Huang
Department of Engineering Science, University of Oxford, Parks Road Oxford, OX1 3PJ, U.K.

(Received 14 August 1996 and in revised form 28 January 1997)

This paper extends the exact theory for second-order wave diffraction by a vertical cylinder in monochromatic waves to the case of bichromatic incident waves. On the basis of the usual assumption of an irrotational flow, the wave-diffraction problems at second-order sum-frequencies and difference-frequencies are considered. The corresponding second-order diffraction potentials are decomposed into three parts; these are associated with the second-order incident wave, the quadratic forcing terms on the free-surface due to the first-order potential, and the linearized 'free-wave' component resulting from the boundary condition on the body surface. A semi-analytical method is presented for obtaining a particular solution which exactly satisfies the inhomogeneous free-surface condition. In the case of a bottom-seated vertical circular cylinder, complete semi-analytical expressions for the second-order sum and difference frequency potentials are derived. Numerical results for the quadratic transfer functions of the second-order force components, and the nonlinear free-surface elevation complete to second-order, are given for this case.

1. INTRODUCTION

It is well known that second-order wave loads may play a significant role in exciting responses of certain types of offshore structure in the frequency ranges either significantly higher or significantly lower than the frequency at which the incident wave possesses most energy. Typical examples of these responses are the low-frequency horizontal-plane motions of moored ships and the high-frequency 'springing' vibrations of ship hulls and tension leg platforms [e.g. Herfjord & Nielsen (1986), Kim & Yue (1988) Eatock Taylor (1991)]. As mentioned by Lee *et al.* (1991), tension leg platforms (TLPs) offer a unique example where both low- and high-frequency second-order forces are important. Furthermore, another major concern for designers is that the nonlinear wave diffraction by a structure may have an even more significant effect on the wave field in the vicinity of the structure. In the case of diffraction of monochromatic incident waves by a single bottom-seated vertical circular cylinder, it has been shown (Kriebel 1992) that the experimental data for maximum wave run-up differ from the predictions of linear theory by up to 44%. Great improvement can be achieved in the theoretical predictions by incorporating the second-order contribution (Kriebel 1992; Huang & Eatock Taylor 1996).

There has therefore been considerable interest in investigating the second-order interactions between waves and structures. The theoretical analysis of this nonlinear phenomenon is usually carried out in the frequency domain. In principle this can be based on directly solving for the second-order velocity potential. For general

0889–9746/97/050465 + 20 $25.00/fl970091

geometries this approach requires a numerical implementation, for example by using a boundary-element method (BEM) [e.g. Chau (1989), Kim & Yue (1989, 1990); Chen *et al.* (1991), Lee *et al.* (1991)]. A disadvantage of this direct approach is that the corresponding computer programs usually require large amounts of CPU time and computer storage to run, and sometimes it is difficult to obtain converged results. This is mainly due to the difficulties in evaluating the free-surface integral which is needed to enforce the inhomogeneous free-surface condition.

An alternative approach, which avoids directly solving for the second-order velocity potential, was proposed by Lighthill (1979) for the case of infinite water depth and by Molin (1979) for finite water depth. This can also be implemented in a numerical method for bodies of arbitrary geometry. Such an indirect approach was also used by Eatock Taylor & Hung (1987) in a semi-analytical investigation of the second-order diffraction forces on a vertical cylinder in regular waves, and was extended by Williams and co-authors (Abul-Azm & Williams, 1988, 1989; Ghalayini & Williams 1991; Moubayed & Williams 1994, 1995) to study second-order interactions between waves and single or multiple vertical cylinders. In the latter case the plane-wave (large-spacing) approximation of McIver & Evans (1984) was adopted. With the indirect approach, however, the difficulties associated with the free-surface integral still exist, and it cannot provide results for the wave run-up and free-surface elevation.

Recently, Newman (1996) investigated the asymptotic behaviour of second-order diffraction of monochromatic waves by a vertical cylinder at both low and high wave frequencies. In Huang & Eatock Taylor (1996) we developed a complete semi-analytical solution for second-order diffraction of monochromatic waves by a truncated vertical cylinder. The latter solution was based on directly solving the boundary-value problem for the first- and second-order velocity potentials. A particular solution to the second-order diffraction potential, exactly satisfying the inhomogeneous free-surface condition, was derived. That solution is here extended to the case of bichromatic incident waves. Both second-order sum- and difference-frequency problems are considered. The second-order diffraction potential for either the sum-frequency or the difference-frequency problem is decomposed into two parts, corresponding to the second-order incident wave and the quadratic forcing on the free-surface (the ''locked'' wave). The eventual purpose of the present approach is to provide an efficient means for predicting second-order loads and free-surface elevations for some offshore structures such as TLPs in irregular waves. The solution for the locked wave component developed here is suitable for arbitrary axisymmetric structures, but for simplicity we restrict the following analysis to the case of a single, bottom-seated vertical circular cylinder. A complete semi-analytical solution is found, thus providing a way of testing the various numerical methods. This solution is more general than that given in the appendix of Kim & Yue (1990), which can only give results for forces. By incorporating an appropriate interaction theory, the present solution can be extended to study the second-order interaction between waves and multiple cylinders.

2. FORMULATION OF THE FIRST- AND SECOND-ORDER VELOCITY POTENTIALS

We consider the diffraction of a plane bichromatic incident wave by a bottom-seated vertical circular cylinder in water of uniform depth h. Assuming irrotational flow, we define the velocity potential of the wave field, $\Phi(r, \theta, z, t)$, in a cylindrical polar coordinate system. The z-axis coincides with the cylinder axis, originating from the

series with respect to the wave slope parameter ε ($\varepsilon \ll 1$):

$$\begin{aligned}\Phi(r, \theta, z, t) &= \varepsilon\Phi^{(1)} + \varepsilon^2\Phi^{(2)} + \mathcal{O}(\varepsilon^3)\\ &= \Re\Big\{\sum_{j=1}^{2} \phi_j^{(1)}(r, \theta, z)\mathrm{e}^{-\mathrm{i}\omega_j t} + \sum_{j=1}^{2}\sum_{l=1}^{2} [\phi_{jl}^{-}(r, \theta, z)\mathrm{e}^{-\mathrm{i}\omega_{jl}^{-}t}\\ &\quad + \phi_{jl}^{+}(r, \theta, z)\mathrm{e}^{-\mathrm{i}\omega_{jl}^{+}t}\Big\} + \mathcal{O}(\varepsilon^3),\end{aligned} \tag{1}$$

where $\omega_{jl}^{\pm} = \omega_j \pm \omega_l$, and ω_j is the angular frequency of the jth wave component ($j = 1,2$).

The first-order potential $\phi_j^{(1)}$ can be written as

$$\phi_j^{(1)} = \sum_{n=0}^{\infty} \varepsilon_n\{\phi_{Ij,n}^{(1)}(r, z) + \phi_{Dj,n}^{(1)}(r, z)\}\cos(n\theta), \tag{2}$$

where $\phi_{Ij,n}^{(1)}$ and $\phi_{Dj,n}^{(1)}$ are, respectively, the nth Fourier harmonics of the first-order incident and diffraction potentials $\phi_{Ij}^{(1)}$ and $\phi_{Dj}^{(1)}$ corresponding to wavenumber k_j, and $\varepsilon_0 = 1$, $\varepsilon_n = 2$ for $n \geq 2$. Furthermore,

$$\phi_{Ij,n}^{(1)}(r, z) = \frac{-\mathrm{i}gA_j}{\omega_j}\frac{\cosh(k_j(z + h))}{\cosh k_j h}\mathrm{J}_n(k_j r)\mathrm{i}^n, \tag{3}$$

where g is the gravitational acceleration, and A_j is the wave amplitude.

We decompose the second-order sum- and difference-frequency potentials $\phi_{jl}^{\pm}$ into

$$\phi^{\pm} = \sum_{n=0}^{\infty} \varepsilon_n\{\phi_{In}^{\pm}(r, z) + \phi_{Dn}^{\pm}(r, z)\}\cos(n\theta), \tag{4}$$

where $\phi_{In}^{\pm}$, $\phi_{Dn}^{\pm}$ are, respectively, the nth Fourier mode of the sum- and difference-frequency incident and diffraction potentials [see also Kim & Yue (1990)], and the subscripts j and l on the sum and difference frequency quantities are here omitted for convenience. $\phi_{In}^{\pm}$ are given by

$$\phi_{In}^{\pm}(r, z) = \frac{1}{2}(\gamma_{jl}^{\pm} + \beta_{lj}^{\pm})\frac{\cosh(k^{\pm}(z + h))}{\cosh k^{\pm}h}\mathrm{J}_n(k^{\pm}r)\mathrm{i}^n, \tag{5}$$

$$\gamma_{jl}^{+} = \frac{-\mathrm{i}gA_jA_l}{2\omega_j}\frac{k_j^2(1 - \tanh^2 k_j h) + 2k_jk_l(1 - \tanh k_j h \tanh k_l h)}{\nu^{+} - k^{+}\tanh k^{+}h}, \tag{6}$$

$$\gamma_{jl}^{-} = \frac{-\mathrm{i}gA_jA_l^{*}}{2\omega_j}\frac{k_j^2(1 - \tanh^2 k_j h) - 2k_jk_l(1 + \tanh k_j h \tanh k_l h)}{\nu^{-} - k^{-}\tanh k^{-}h}, \tag{7}$$

$$\beta_{lj}^{+} = \gamma_{lj}^{+}, \qquad \beta_{lj}^{-} = \gamma_{lj}^{-}{}^{*}, \qquad k^{\pm} = k_j \pm k_l, \qquad \nu^{\pm} = \omega^{\pm 2}/g,$$

where an asterisk denotes the complex conjugate. The asymptotic behavior of ϕ_I^{+} and ϕ_I^{-}, which are the summation of the corresponding Fourier components, is discussed by Kim & Yue (1990).

The sum- and difference-frequency diffraction potentials $\phi_D^{\pm}(r, \theta, z)$ satisfy the following boundary-value problem:

$$\nabla^2\phi_D^{\pm} = 0, \qquad (r, \theta, z) \in \Omega; \tag{8}$$

$$\frac{\partial\phi_D^{\pm}}{\partial z} - \nu^{\pm}\phi_D^{\pm} = q^{\pm}(r, \theta), \qquad z = 0, \tag{9}$$

$$\frac{\partial\phi_D^{\pm}}{\partial z} = 0, \qquad z = -h, \qquad \frac{\partial\phi_D^{\pm}}{\partial n} = -\frac{\partial\phi_I^{\pm}}{\partial n}, \quad \text{on } S_B, \tag{10}$$

where Ω is the quiescent fluid domain, and $q^{\pm}(r, \theta)$ are the sum- and difference-frequency forcing terms on the free-surface, defined by

$$q^{+} = \tfrac{1}{2}(q_{jl}^{+} + q_{lj}^{+}), \qquad q^{-} = \tfrac{1}{2}(q_{jl}^{-} + q_{lj}^{-}*). \tag{11}$$

The sum frequency forcing term is obtained from

$$\begin{aligned} q_{jl}^{+} = {} & \frac{\mathrm{i}\omega_l k_j^2}{2g}(\phi_{Dj}^{(1)}\phi_{Dl}^{(1)})(3\tanh^2 k_j h - 1) + \frac{\mathrm{i}\omega_l}{g}\left[\frac{\partial\phi_{Dj}^{(1)}}{\partial r}\frac{\partial\phi_{Dl}^{(1)}}{\partial r} + \frac{1}{r^2}\frac{\partial\phi_{Dj}^{(1)}}{\partial\theta}\frac{\partial\phi_{Dl}^{(1)}}{\partial\theta}\right] \\ & + \frac{2\mathrm{i}\omega_l}{g}\left[\frac{\partial\phi_{Ij}^{(1)}}{\partial r}\frac{\partial\phi_{Dl}^{(1)}}{\partial r} + \frac{1}{r^2}\frac{\partial\phi_{Ij}^{(1)}}{\partial\theta}\frac{\partial\phi_{Dl}^{(1)}}{\partial\theta}\right] \\ & + \frac{\mathrm{i}\omega}{g}(\phi_{Il}^{(1)}\phi_{Dj}^{(1)})k_j^2\left(\tanh^2 k_j h + \frac{2k_l}{k_j}\tanh k_j h \tanh k_l h - 1\right), \end{aligned} \tag{12}$$

after the free-surface boundary conditions for $\phi_{Dj}^{(1)}$, $\phi_{Dl}^{(1)}$ have been exploited. One can get the expression for q_{jl}^{-} by replacing $\mathrm{i}\omega_l$ with $-\mathrm{i}\omega_l$, and $\phi_{Il}^{(1)}$, $\phi_{Dl}^{(1)}$ and their derivatives with the corresponding complex conjugates. Apart from the above governing equation and boundary conditions, $\phi_D^{\pm}$ should satisfy appropriate radiation conditions at $r \to \infty$, which will be discussed in Sections 3 and 4.

3. SOLUTION OF THE SECOND ORDER DIFFRACTION POTENTIALS

3.1. Decomposition of the Potentials into Components

We decompose the sum- and difference-frequency diffraction potentials $\phi_D^{\pm}(r, \theta, z)$ into two components:

$$\phi_D^{\pm}(r, \theta, z) = \phi_{1D}^{\pm} + \phi_{2D}^{\pm}, \tag{13}$$

where $\phi_{1D}^{\pm}$ corresponds to the free wave potentials due to linear diffraction of the second-order incident wave, and $\phi_{2D}^{\pm}$ are the locked waves due to the forcing terms on the free surface, satisfying a homogeneous condition on the body surface.

We further expand $\phi_{kD}^{\pm}$, $k = 1,2$ into Fourier series:

$$\phi_{kD}^{\pm} = \sum_{n=0}^{\infty} \varepsilon_n \phi_{kD,n}^{\pm} \cos n\theta. \tag{14}$$

Each of the above components satisfies the following Helmholtz equation in the fluid domain and the common boundary condition on the seabed $z = -h$:

$$\frac{\partial^2\phi_{kD,n}^{\pm}}{\partial r^2} + \frac{1}{r}\frac{\partial\phi_{kD,n}^{\pm}}{\partial r} + \frac{\partial^2\phi_{kD,n}^{\pm}}{\partial z^2} = \frac{n^2}{r^2}\phi_{kD,n}^{\pm}, \quad (r, \theta, z) \in \Omega; \tag{15}$$

$$\frac{\partial\phi_{kD,n}^{\pm}}{\partial z} = 0, \qquad z = -h. \tag{16}$$

On the quiescent free surface, the boundary condition can be specified as

$$\frac{\partial\phi_{kD,n}^{\pm}}{\partial z} - \nu^{\pm}\phi_{kD,n}^{\pm} = \delta_k q_n^{\pm}(r, \theta), \quad z = 0, \tag{17}$$

where $\delta_k = 0$ for $k = 1$, and $\delta_k = 1$ for $k = 2$; $q_n^{\pm}$ are the nth Fourier harmonics of the free-surface forcing terms, i.e.

$$q_n^{+} = \tfrac{1}{2}(q_{jl,n}^{+} + q_{lj,n}^{+}), \quad q_n^{-} = \tfrac{1}{2}(q_{jl,n}^{-} + q_{lj,n}^{-*}). \tag{18}$$

By expanding the first-order incident and diffraction potentials into Fourier components, we can get the following expressions for $q_{jl,n}^{+}$:

$$\begin{aligned} q_{jl,n}^{+} = \varepsilon_n c_2 \sum_{m=n}^{\infty} \Bigg\{ & \left(\frac{\partial \phi_{Dj,m}^{(1)}}{\partial r}\right)\left(\frac{\partial \phi_{Dl,n-m}^{(1)}}{\partial r}\right) + \left[\frac{m(n-m)}{r^2} + c_1\right][\phi_{Dj,m}^{(1)}\phi_{Dl,n-m}^{(1)}] \\ & + \left[\left(\frac{\partial \phi_{Ij,m}^{(1)}}{\partial r}\right)\left(\frac{\partial \phi_{Dl,n-m}^{(1)}}{\partial r}\right) + \left(\frac{\partial \phi_{Ij,n-m}^{(1)}}{\partial r}\right)\left(\frac{\partial \phi_{Dl,m}^{(1)}}{\partial r}\right)\right] + \left[\frac{m(n-m)}{r^2} + c_3\right] \\ & \times [\phi_{Dj,n-m}^{(1)}\phi_{Il,m}^{(1)} + \phi_{Il,n-m}^{(1)}\phi_{Dj,m}^{(1)}]\Bigg\} + c_2 \sum_{m=0}^{n} \Bigg\{ \left(\frac{\partial \phi_{Dj,m}^{(1)}}{\partial r}\right)\left(\frac{\partial \phi_{Dl,n-m}^{(1)}}{\partial r}\right) \\ & + \left[c_1 - \frac{m(n-m)}{r^2}\right][\phi_{Dj,m}^{(1)}\phi_{Dl,n-m}^{(1)}] + 2\left(\frac{\partial \phi_{Ij,m}^{(1)}}{\partial r}\right)\left(\frac{\partial \phi_{Dl,n-m}^{(1)}}{\partial r}\right) \\ & + 2\left[c_3 - \frac{m(n-m)}{r^2}\right](\phi_{Dl,n-m}^{(1)})(\phi_{Ij,m}^{(1)})\Bigg\}, \end{aligned} \tag{19}$$

where

$$c_1 = -\tfrac{1}{2}k_j^2(1 - 3\tanh^2 k_j h), \qquad c_2 = -\frac{\mathrm{i}A_j A_l g}{2\omega_j}, \tag{20}$$

$$c_3 = \tfrac{1}{2}k_j^2\left(\tanh^2 k_j h + 2\frac{k_j}{k_j}\tanh k_j h \tanh k_l h - 1\right). \tag{21}$$

One can obtain the equation for $q_{jl,n}^{-}$ by replacing $-\mathrm{i}$ with i in the expression for c_2, and replacing all the incident and diffraction potentials and their derivatives which correspond to wavenumber k_l with the corresponding complex conjugates.

3.2. Solution for $\phi_{1D,n}^{\pm}$

Apart from the governing Helmholtz equation and the common boundary conditions at the sea bottom and on the free-surface [equations (15)–(17)], we need to specify the radiation condition at $r \to \infty$ and the boundary condition on $r = a$ for $\phi_{1D,n}^{\pm}$. We first separate the variables r and z using the eigenfunction expansion method. We write

$$\phi_{1D,n}^{\pm} = \sum_{m=0}^{\infty} P_{mn}^{\pm}(r) Z_m^{\pm}(z), \tag{22}$$

where

$$Z_0^{\pm}(z) = \frac{1}{\sqrt{N_0^{\pm}}}\cosh(k_0^{\pm}(z+h)), \quad N_0^{\pm} = \frac{h}{2}\left(1 + \frac{\sinh(2k_0^{\pm}h)}{2k_0^{\pm}h}\right), \tag{23}$$

$$Z_m^{\pm}(z) = \frac{1}{\sqrt{N_n^{\pm}}}\cos(k_m^{\pm}(z+h)), \quad N_m = \frac{h}{2}\left(1 + \frac{\sin(2k_m^{\pm}h)}{2k_m^{\pm}h}\right), \qquad m > 0. \tag{24}$$

$k_0^{\pm}$ is the real root of the dispersion equation (25) and $k_m^{\pm}$ ($m = 1, 2, \ldots$) are the real roots of dispersion equation (26) below:

$$k_0^{\pm}\tanh k_0^{\pm}h = \nu^{\pm}, \tag{25}$$

$$k_m^{\pm}\tan(k_m^{\pm}h) = -\nu^{\pm}. \tag{26}$$

By substituting equation (22) into (15), one can obtain the governing equation for $P^{\pm}_{mn}(r)$, which is the ordinary Bessel equation for $m = 0$ and the modified Bessel equation for $m > 0$. Each component $P^{\pm}_{mn}$ must, of course, satisfy the Sommerfeld radiation condition. Thus, we have

$$\lim_{r\to\infty} \sqrt{r}\left(\frac{\mathrm{d}P^{\pm}_{mn}}{\mathrm{d}r} - \mathrm{i}k^{\pm}_m P^{\pm}_{mn}(r)\right) = 0, \qquad m = 0, 1, 2, \ldots \tag{27}$$

Furthermore, we specify the boundary condition on the surface of the cylinder, $r = a$, as

$$\frac{\partial \phi^{\pm}_{1D,n}}{\partial r} = -\frac{\partial \phi^{\pm}_{In}}{\partial r}. \tag{28}$$

Solutions to the Bessel equation ($m = 0$) and modified Bessel equation ($m > 0$) which satisfy the radiation condition at $r \to \infty$ are of the form:

$$P^{\pm}_{mn}(r) = \begin{cases} \alpha^{\pm}_0 \mathrm{H}_n(k^{\pm}_0 r)/H'_n(k^{\pm}_0 a) & m = 0 \\ \alpha^{\pm}_m \mathrm{K}_n(k^{\pm}_m r)/K'_n(k^{\pm}_m a) & m > 0 \end{cases}$$

where $\mathrm{H}_n(x)$ is the nth order Hankel function of the first kind, $\mathrm{K}_n(x)$ is the nth order modified Bessel function, and a prime denotes the derivative with respect to the argument; $\alpha^{\pm}_0$, $\alpha^{\pm}_m$ are constants which are determined from equation (28) as

$$\alpha^{\pm}_0 = \frac{k^{\pm}\sinh(k^{\pm}h) + \nu^{\pm}\cosh(k^{\pm}h)}{k^{\pm 2} - k^{\pm 2}_0}\frac{E^{\pm}_n Z^{\pm}_0(0)}{k^{\pm}_0}, \tag{29}$$

$$\alpha^{\pm}_m = \frac{k^{\pm}\sinh(k^{\pm}h) - \nu^{\pm}\cosh(k^{\pm}h)}{k^{\pm 2} + k^{\pm 2}_0}\frac{E^{\pm}_n Z^{\pm}_m(0)}{k^{\pm}_m}, \tag{30}$$

$$E^{\pm}_n = -\tfrac{1}{2}(\beta^{\pm}_{jl} + \gamma^{+}_{lj})\frac{k^{\pm}\mathrm{J}'_n(k^{\pm}a)}{\cosh k^{\pm}h}\varepsilon_n \mathrm{i}^n. \tag{31}$$

3.3. Solution for $\phi^{\pm}_{2D,n}$ in the Case of Finite Water Depth

Using the Fourier expansion in the circumferential direction and the eigenfunction expansion in the vertical direction, we can express $\phi^{\pm}_{2D,n}$ in the following form:

$$\phi^{\pm}_{2D,n}(r, \theta, z) = \varepsilon_n \frac{\cosh(k^{\pm}(z+h))}{\nu^{\pm}\cosh(k^{\pm}h)} q^{\pm}_n(r) + \sum_{m=0}^{\infty} \varepsilon_n R^{\pm}_{mn}(r) Z^{\pm}_m(z). \tag{32}$$

One can easily check that if we take the wave number $\kappa^{\pm}$ in the above equation as the real root of the dispersion equation

$$\kappa^{\pm}\tanh(\kappa^{\pm}h) = 2\nu^{\pm} \tag{33}$$

then the inhomogeneous boundary condition on the free-surface is exactly satisfied. The vertical eigenfunctions $Z^{\pm}_m(z)$ have been defined in equations (23) and (24). Substituting equation (32) into (15), and using the eigenfunction expansion approach, one can derive the following governing equation for $R^{\pm}_{mn}(r)$:

$$\frac{\mathrm{d}^2 R^{\pm}_{mn}}{\mathrm{d}r^2} + \frac{1}{r}\frac{\mathrm{d}R^{\pm}_{mn}}{\mathrm{d}r} + \left(\sigma_m k^{\pm 2}_m - \frac{n^2}{r^2}\right)R^{\pm}_{mn} + A^{\pm}_m\left[\frac{\mathrm{d}^2 q^{\pm}_n}{\mathrm{d}r^2} + \frac{1}{r}\frac{\mathrm{d}q^{\pm}_n}{\mathrm{d}r} + \left(\kappa^{\pm 2} - \frac{n^2}{r^2}\right)q^{\pm}_n\right] = 0, \tag{34}$$

where

$$A_m^{\pm} = \int_{-h}^{0} \frac{\cosh \kappa^{\pm}(z+h)}{\nu^{\pm} \cosh(\kappa^{\pm} h)} Z_m^{\pm}(z)\, \mathrm{d}z \tag{35}$$

and $\sigma_m = 1$ for $m = 0$, $\sigma_m = -1$ for $m > 0$. By integrating and using the dispersion relationships for $k_0^{\pm}$ and $k_m^{\pm}$, we obtain:

$$A_0^{\pm} = \frac{\cosh(k_0^{\pm} h)}{\sqrt{N_0^{\pm}}(\kappa^{\pm 2} - k_0^{\pm 2})} = \frac{Z_0^{\pm}(0)}{\kappa^{\pm 2} - k_0^{\pm 2}}, \quad A_m^{\pm} = \frac{\cos(k_m^{+} h)}{\sqrt{N_m^{\pm}}(\kappa^{\pm 2} + k_m^{\pm 2})} = \frac{Z_m^{\pm}(0)}{\kappa^{\pm 2} + k_m^{\pm 2}}.$$

The governing equations for $R_{mn}^{\pm}(r)$ are now inhomogeneous, with the homogeneous part (when all the A_m are equal to zero) being the Bessel equation (for $m = 0$) and the modified Bessel equation (for $m > 0$). As described in section 3.2, one can use the Sommerfeld condition to specify the behavior as $r \to \infty$. The final boundary condition needed is that at $r = a$, namely

$$\frac{\mathrm{d}R_{mn}^{\pm}(a)}{\mathrm{d}r} = 0. \tag{36}$$

The exact solution to the inhomogeneous ordinary differential equation (34), subject to homogeneous boundary conditions at $r = a$ and $r = b(\to \infty)$ can be readily written [as described in detail for the monochromatic case by Huang & Eatock Taylor (1996)]:

$$R_{mn}^{\pm}(r) = A_m^{\pm}(\kappa^{\pm 2} + \sigma_m k_m^{\pm 2}) \int_a^{\infty} \xi q_n^{\pm}(\xi) G_{mn}^{\pm}(r, \xi)\, \mathrm{d}\xi - A_m^{\pm} q_n^{\pm}(r). \tag{37}$$

Here $G_{mn}^{\pm}(r, \xi)$ are the Green's functions, which are given by

$$G_{0n}^{\pm}(r, \xi) = \begin{cases} \mathrm{i}\pi \mathrm{H}_n(k_0^{\pm}\xi)[\mathrm{J}_n(k_0^{\pm} r) - h_0^{\pm}(n)\mathrm{H}_n(k_0^{\pm} r)]/2, & r < \xi \\ \mathrm{i}\pi \mathrm{H}_n(k_0^{\pm} r)[\mathrm{J}_n(k_0^{\pm}\xi) - h_0^{\pm}(n)\mathrm{H}_n(k_0^{\pm}\xi)]/2, & r > \xi, \end{cases} \tag{38}$$

$$G_{mn}^{\pm}(r, \xi) = \begin{cases} \mathrm{K}_n(k_m^{\pm}\xi)[\mathrm{I}_n(k_m^{\pm} r) - h_m^{\pm}(n)\mathrm{K}_n(k_m^{\pm} r)], & r < \xi \\ \mathrm{K}_n(k_m^{\pm} r)[\mathrm{I}_n(k_m^{\pm}\xi) - h_m^{\pm}(n)\mathrm{K}_n(k_m^{\pm}\xi)], & r > \xi, \end{cases} \tag{39}$$

where

$$h_0^{\pm}(n) = \mathrm{J}_n'(k_0^{\pm} a)/\mathrm{H}_n'(k_0^{\pm} a), \tag{40}$$

$$h_m^{\pm}(n) = \mathrm{I}_n'(k_m^{\pm} a)/\mathrm{K}_n'(k_m^{\pm} a). \tag{41}$$

As discussed in Huang & Eatock Taylor (1996), to the zeroth order of continuity in $\phi_{2D}^{\pm}$, the second term on the right-hand side of equation (37), multiplied by ε_n, would cancel out the first term on the right-hand side of equation (32), and therefore $\phi_{2D}^{\pm}$ is reduced to the simpler form, $\phi_{2D0}^{\pm}$, given by

$$\phi_{2D0}^{\pm}(r, \theta, z) = \sum_{n=0}^{\infty} \varepsilon_n \cos(n\theta) \left\{ \sum_{m=0}^{\infty} Z_m^{\pm}(0) Z_m^{\pm}(z) \int_a^{\infty} \xi q_n^{\pm}(\xi) G_{mn}^{\pm}(r, \xi)\, \mathrm{d}\xi \right\}. \tag{42}$$

Here subscript 0 refers to C^0 continuity. This expression is simple and semi-analytical, and is in fact of a sufficiently general form to provide a particular solution for the diffraction of bichromatic waves by any vertical axisymmetric structure having a radius a at the waterline. The C^0 order of continuity is sufficient to yield accurate results for second-order forces, wave run-up and free-surface elevation.

In numerical implementation, the line integral in equation (42) can conveniently be divided into two parts: a near-field part which accounts for the contribution of the evanescent waves, and a far-field part in which the local waves are neglected. The first part is evaluated by numerical quadrature, and the second part is integrated analytically by adopting the asymptotic forms of the associated Hankel functions. Details of this approach can be found in Kim & Yue (1989), and Chau & Eatock Taylor (1992).

3.4. The Expression for $\phi^{\pm}_{2D,n}$ in Infinite Water Depth

The methodology for obtaining the second-order particular solution for the sum and difference potentials presented in Section 3.3 is also suitable for extending the solution to the infinite water depth case, in which the second-order sum- and difference-frequency incident and diffraction potentials vanish. In this case the general expression for the particular solution in equation (32) is changed into

$$\phi^{\pm}_{2D,n}(r, z) = \varepsilon_n \frac{\exp(2\nu^{\pm} z)}{\nu^{\pm}} q^{\pm}_n(r) + \varepsilon_n \left\{ R^{\pm}_{0n}(r) Z^{\pm}_0(z) + \int_0^{\infty} R^{\pm}_n(\mu r) Z^{\pm}(\mu, z)\, \mathrm{d}\mu \right\}, \quad (43)$$

where the eigenvalue μ belongs to a continuous spectrum. $Z^{\pm}_0(z)$ and $Z^{\pm}(\mu, z)$ are now the normalized eigenfunctions

$$Z^{\pm}_0(z) = \sqrt{2\nu^{\pm}} \mathrm{e}^{\nu^{\pm} z}, \quad (44)$$

$$Z(\mu, z) = \sqrt{\frac{2}{\pi(\mu^2 + \nu^{\pm 2})}} [\mu \cos(\mu z) + \nu^{\pm} \sin(\mu z)]. \quad (45)$$

By using the same procedures as described in Section 3.3 we can derive expressions for $R^{\pm}_{0n}$, $R^{\pm}_n(\mu, r)$, which are similar to those for the case of finite water depth. We thereby obtain the complete expression for $\phi^{\pm}_{2D,n}$:

$$\begin{aligned} \phi^{\pm}_{2D,n} = \varepsilon_n \Bigg\{ & Z^{\pm}_0(0) Z^{\pm}_0(z) \int_a^{\infty} \xi q^{\pm}_n(\xi) G^{\pm}_{0n}(r, \xi)\, \mathrm{d}\xi \\ & + \int_0^{\infty} Z^{\pm}(\mu, 0) Z^{\pm}(\mu, z) \int_a^{\infty} \xi q^{\pm}_n(\xi) G_n(\mu r, \mu\xi)\, \mathrm{d}\xi\, \mathrm{d}\mu + \frac{\exp(2\nu^{\pm} z)}{\nu^{\pm}} q^{\pm}_n(r) \\ & - \left[\frac{\sqrt{2}\, Z^{\pm}_0(z)}{3\nu^{\pm}\sqrt{\nu^{\pm}}} + \int_0^{\infty} \left(\int_{-\infty}^{0} \frac{\exp(2\nu^{\pm} z) Z^{\pm}(\mu, z)}{\nu^{\pm}} \mathrm{d}z \right) Z^{\pm}(\mu, z)\, \mathrm{d}\mu \right] q^{\pm}_n(r) \Bigg\}. \end{aligned} \quad (46)$$

The expression for $G^{\pm}_{0n}(r, \xi)$ is the same as that in the finite water depth case, while $G_n(\mu r, \mu\xi)$ is slightly modified, the difference being that $k^{\pm}_m$ should be replaced by μ. To the zeroth-order of continuity, the potential $\phi^{\pm}_{2D,n}$ for infinite depth can be expressed as

$$\begin{aligned} \phi^{\pm}_{2D,n} = \varepsilon_n \Bigg[& Z^{\pm}_0(0) Z^{\pm}_0(z) \int_a^{\infty} \xi q^{\pm}_n(\xi) G^{\pm}_{0n}(r, \xi)\, \mathrm{d}\xi \\ & + \int_0^{\infty} Z^{\pm}(\mu, 0) Z^{\pm}(\mu, z) \int_a^{\infty} \xi q^{\pm}_n(\xi) G_n(\mu r, \mu\xi)\, \mathrm{d}\xi\, \mathrm{d}\mu \Bigg]. \end{aligned} \quad (47)$$

This is seen to be analogous to the finite water depth case.

4. QUADRATIC TRANSFER FUNCTIONS (QTFs)

By using the same perturbation procedure as for the second-order potential, one can also express the pressure $p(t)$, the free-surface elevation $\zeta(t)$, and the total force $\mathbf{F}(t)$ and moment $\mathbf{M}(t)$ as perturbation series in ε. The associated first- and second-order terms are given by:

$$[p^{(1)}(t),\, \zeta^{(1)}(t)] = \left[-\rho \frac{\partial \phi^{(1)}}{\partial t},\ -\frac{1}{g}\frac{\partial \phi^{(1)}}{\partial t}\bigg|_{z=0}\right], \tag{48}$$

$$[p^{(2)}(t),\, \zeta^{(2)}(t)] = \left[-\rho \frac{\partial \phi^{(2)}}{\partial t} - \frac{1}{2}\rho(\nabla\phi^{(1)})^2,\right.$$

$$\left. -\frac{1}{2g}(\nabla\phi^{(1)})^2 + \frac{1}{g^2}\frac{\partial \phi^{(1)}}{\partial t}\frac{\partial^2 \phi^{(1)}}{\partial t\, \partial z} - \rho \frac{\partial \phi^{(2)}}{\partial t}\bigg|_{z=0}\right]. \tag{49}$$

When $p(t)$ is known, the total force and moment can be obtained by integrating over the wetted body surface. In the following, we define $\mathbf{M}(t)$ as the moment about the seabed.

The second-order free-surface elevation, forces and moments can be expressed as:

$$[\zeta, \mathbf{F}, \mathbf{M}] = \Re \sum_{j=1}^{2}\sum_{l=1}^{2} \left\{ \left[\frac{A_j A_l}{a}\eta_{jl}^{+},\quad \rho g a A_j A_l \mathbf{F}_{jl}^{+},\quad \rho g a h A_j A_l \mathbf{M}_j^{+}\right] e^{-i\omega^{+}t}\right.$$

$$\left. + \left[\frac{A_j A_l^{*}}{a}\eta_{jl}^{-},\ \rho g a A_j A_l \mathbf{F}_{jl,}^{-}\quad \rho g a h A_j A_l \mathbf{M}_{jl}^{-}\right] e^{-i\omega^{-}t}\right\}. \tag{50}$$

$\eta_{jl}^{\pm}$, $\mathbf{F}_{jl}^{\pm}$, and $\mathbf{M}_{jl}^{\pm}$ are the quadratic transfer functions defined respectively for $\zeta(t)$, $\mathbf{F}(t)$ and $\mathbf{M}(t)$, which can be split into separate contributions from quadratic effects from the first order potentials (subscript q), and contributions from the second order potentials (subscript p). Thus

$$[\eta_{jl}^{\pm},\quad \mathbf{F}_{jl}^{\pm},\quad \mathbf{M}_{jl}^{\pm}] = [\eta_{jlq}^{\pm},\quad \mathbf{F}_{jlq}^{\pm},\quad \mathbf{M}_{jlq}^{\pm}] + [\eta_{jlp}^{\pm},\quad \mathbf{F}_{jlp}^{\pm},\quad \mathbf{M}_{jlp}^{\pm}]. \tag{51}$$

As a result of the simple geometry, we can derive analytical expressions for the quadratic components of the surge and pitch force QTFs as follows:

$$[F_{x,jlq}^{\pm},\quad M_{y,jlq}^{\pm}] = \pm \frac{2i}{\pi(k_j a)(k_l a)}\sum_{n=0}^{\infty}(-1)^n \Omega_{njl}^{\pm}\left[1 \quad \pm \frac{g k_j k_l h}{\omega_j \omega_l}\frac{I_{F,M}^{-} + I_{F,M}^{+} n(n+1)/(k_j k_l a^2)}{\cosh k_j h \cosh k_l h}\right], \tag{52}$$

where, as before, the $\pm$ sign is $+$ for the sum-frequency problems and $-$ for the difference-frequency problems. $I_F^{\pm}$ is for the surge force and $I_M^{\pm}$ is for the pitch moment, defined by

$$I_F^{\pm} = \frac{\sinh k^{+}h}{2k^{+}h} \pm \frac{\sinh k^{-}h}{2k^{-}h}, \tag{53}$$

$$I_M^{\pm} = \frac{1}{2}\left[\frac{\sinh k^{+}h}{k^{+}h} - \frac{\cosh(k^{+}h) - 1}{(k^{+}h)^2} \pm \left(\frac{\sinh k^{-}h}{k^{-}h} - \frac{\cosh(k^{-}h) - 1}{(k^{-}h)^2}\right)\right]. \tag{54}$$

Furthermore,

$$\Omega^{+}_{njl} = \frac{1}{H'_{n+1}(k_j a)H'_n(k_l a)} + \frac{1}{H'_n(k_j a)H'_{n+1}(k_l a)}, \tag{55}$$

$$\Omega^{-}_{njl} = \frac{1}{H'_{n+1}(k_j a)H'^{*}_n(k_l a)} - \frac{1}{H'_n(k_j a)H'^{*}_{n+1}(k_l a)}. \tag{56}$$

5. NUMERICAL RESULTS

5.1. Comparison of QTFs with Existing Results

In testing the method presented in this paper, and the associated numerical algorithms, we have first considered the surge force QTFs for two cases for which other published QTF data are available. These correspond to $h/a = 1$ and $h/a = 4$, respectively.

Table 1 gives results for components of sum-frequency surge force QTF, for the case of $h/a = 1$. The upper triangular matrix presents analytical results from the method presented in this paper, and the lower triangle presents Kim & Yue's (1990) numerical results over the same range of the bi-frequency plane. The nondimensional frequencies are defined by $\bar{\nu}_i = \omega_i^2 a/g$, $i = j, l$. At each frequency pair, results are tabulated for the magnitude of the quadratic force due to the first order potentials, $|F^{\pm}_{x,jlq}|$; the force due to the sum frequency potential $|F^{\pm}_{x,jlp}|$; and the total second order force $|F^{\pm}_{x,jl}|$. Kim & Yue's results were obtained from a ring source boundary element analysis, which yields

Table 1

Magnitudes of the components of second-order sum-frequency surge force QTF on a vertical circular cylinder, for $h/a = 1$. The upper right triangle contains our present analytical results, and the lower triangle contains Kim & Yue's results. The values shown are: first row $|F^{\pm}_{x,jlq}|$, second row $|F^{\pm}_{x,jlp}|$, third row $|F^{\pm}_{x,jl}|$

	$\bar{\nu}_j$	1·0	1·2	1·4	1·6	1·8	2·0
$\bar{\nu}_l$							
	1·440 |	1·441	1·578	1·710	1·804	1·832	1·786
1·0	1·636 |	1·639	1·976	2·243	2·645	2·714	2·635
	0·939 |	0·946	0·775	0·769	0·886	0·909	0·855
	1·577	1·676 |	1·677	1·766	1·815	1·801	1·717
1·2	1·963	2·262 |	2·264	2·516	2·744	2·830	2·662
	0·782	0·752 |	0·757	0·829	0·941	1·031	0·955
	1·709	1·764	1·805 |	1·807	1·811	1·758	1·643
1·4	2·308	2·549	2·754 |	2·756	2·831	2·872	2·705
	0·778	0·847	0·971 |	0·972	1·045	1·115	1·062
	1·802	1·813	1·808	1·772 |	1·776	1·695	1·566
1·6	2·582	2·752	2·876	2·930 |	2·931	2·862	2·700
	0·850	0·959	1·074	1·160 |	1·157	1·167	1·135
	1·828	1·797	1·753	1·689	1·593 |	1·602	1·479
1·8	2·710	2·807	2·857	2·872	2·816 |	2·821	2·691
	0·903	1·103	1·105	1·184	1·226 |	1·222	1·211
	1·778	1·709	1·634	1·556	1·467	1 368 |	1·384
2·0	2·661	2·682	2·671	2·668	2·688	2·692 |	2·694
	0·886	0·973	1·037	1·114	1·227	1·334 |	1·322

TABLE 2

Magnitudes of quadratic components of the second-order sum- and difference-frequency surge force QTF for a vertical circular cylinder, for $h/a = 4$. The upper triangle contains results for the sum-frequency problem, and the lower triangle contains results for the difference-frequency problem. The values shown are: first row, present theory; second-row, Kim & Yue (1990); third row, Moubayed & Williams (1995)

	$\bar{\nu}_j$	1·0	1·2	1·4	1·6	1·8	2·0
$\bar{\nu}_l$							
	0·669 |	1·492	1·546	1·682	1·853	1·973	2·001
1·0	0·666 |	1·493	1·546	1·681	1·850	1·969	1·995
	0·666 |	1·494	1·546	1·680	1·851	1·973	2·005
	0·650	0·638 |	1·642	1·775	1·912	1·985	1·965
1·2	0·647	0·636 |	1·641	1·774	1·909	1·981	1·959
	0·648	0·637 |	1·640	1·773	1·911	1·986	1·970
	0·615	0·615	0·606 |	1·870	1·948	1·960	1·884
1·4	0·612	0·612	0·603 |	1·868	1·945	1·957	1·878
	0·614	0·613	0·604 |	1·869	1·949	1·964	1·893
	0·581	0·591	0·597	0·603 |	1·960	1·914	1·793
1·6	0·578	0·588	0·594	0·600 |	1·907	1·910	1·786
	0·581	0·591	0·596	0·602 |	1·964	1·921	1·804
	0·556	0·571	0·586	0·605	0·618 |	1·825	1·685
1·8	0·552	0·567	0·583	0·602	0·615 |	1·820	1·677
	0·559	0·572	0·586	0·604	0·617 |	1·836	1·699
	0·538	0·550	0·570	0·596	0·619	0·627 |	1·554
2·0	0·534	0·547	0·566	0·593	0·615	0·624 |	1·544
	0·544	0·555	0·572	0·598	0·619	0·627 |	1·571

the second-order potential for axisymmetric bodies. Good agreement is found between our results and these published data.

Another set of comparisons, for the components of both sum and difference frequency surge force QTFs, is presented in Tables 2 and 3. These correspond to the case of $h/a = 4$, for which results have been published by both Kim & Yue (1990) and Moubayed & Williams (1995). As mentioned above, Kim & Yue's results were obtained from a direct numerical solution of the second-order potential for axisymmetric bodies. The analysis of Moubayed & Williams used the indirect method to obtain semi-analytical expressions for the second-order forces. These tables are organized in a different manner from Table 1. Now the lower triangle lists the results for the difference-frequency problem, while the upper triangle contains the sum-frequency results. At each frequency pair, three numbers are given, corresponding to our results, those of Kim & Yue, and those of Moubayed & Williams, respectively. The magnitudes of the quadratic forces due to the first-order potentials are given in Table 2, and the total forces in Table 3. We have not listed the forces due to the sum and difference frequency potentials, since there are no directly comparable published results for the latter case. It is clear, however, from the data given in these tables that the results all compare very well. Except for the magnitude of the total surge force QTF at $(\bar{\nu}_j, \bar{\nu}_l) = (2{\cdot}0, 2{\cdot}0)$, all other data are found to be close to those of Kim & Yue and Moubayed & Williams. The cause for the single substantial discrepancy is not clear.

A fuller understanding of the characteristics of the sum and difference frequency surge force QTFs may be gained from contour plots. Figures 1–3 show such plots for the case $h/a = 4$. Each figure contains three contour plots, corresponding to (a) the

TABLE 3

Magnitudes of the total second-order sum and difference frequency surge force QTF for a vertical circular cylinder, for $h/a = 4$. The upper triangle contains results for the sum-frequency problem, and the lower triangle contains results for the difference-frequency problem. The values shown are: first row, present theory; second-row, Kim & Yue (1990); third row, Moubayed & Williams (1995)

	$\bar{\nu}_j$	1·0	1·2	1·4	1·6	1·8	2·0
$\bar{\nu}_i$							
	0·669 |	1·526	1·667	1·749	1·883	1·801	1·681
1·0	0·666 |	1·518	1·641	1·748	1·853	1·809	1·620
	0·666 |	1·466	1·602	1·725	1·783	1·724	1·563
	0·693	0·638 |	2·092	2·298	2·336	2·294	1·798
1·2	0·689	0·636 |	2·084	2·262	2·302	2·182	1·899
	0·686	0·637 |	1·997	2·134	2·225	2·091	1·793
	0·776	0·646	0·606 |	2·621	2·795	2·474	2·114
1·4	0·763	0·640	0·603 |	2·612	2·714	2·505	2·094
	0·751	0·641	0·604 |	2·548	2·630	2·422	1·998
	0·849	0·700	0·616	0·603 |	3·030	2·859	2·372
1·6	0·856	0·701	0·615	0·600 |	3·021	2·935	2·375
	0·840	0·697	0·617	0·602 |	2·910	2·848	2·272
	0·974	0·769	0·680	0·615	0·618 |	3·294	3·001
1·8	0·943	0·788	0·678	0·619	0·615 |	3·277	3·018
	0·913	0·761	0·677	0·622	0·617 |	3·184	2·999
	0·980	0·845	0·777	0·690	0·617	0·627 |	3·507
2·0	1·009	0·877	0·765	0·678	0·629	0·624 |	3·052
	0·992	0·862	0·734	0·676	0·630	0·627 |	3·151

quadratic component, (b) the component based on the sum or difference frequency potential, (c) the total. Figure 1 gives the sum frequency QTFs over the range $1 < \bar{\nu}_i < 2$, $i = 1,2$. It is immediately apparent that the quadratic component does not vary strongly with distance away from the diagonal $\bar{\nu}_1 = \bar{\nu}_2$, but the sum frequency potential component falls off rapidly with this distance at the higher end of the range. Since the latter is substantially larger than the former, it provides the pattern for the total second-order force. This has a ridge along the diagonal, which increases in height with increase in frequency. This behavior is continued at higher frequencies, as shown in Figure 2, which covers the range $2 < \bar{\nu}_i < 3$.

Figure 3 is equivalent to Figure 1, but shows the difference frequency components over this range. The quadratic component in Figure 3(a) is fairly flat, with a route over the pass at $\bar{\nu}_1 = \bar{\nu}_2 = 1{\cdot}5$ in the direction $\bar{\nu}_1 + \bar{\nu}_2 = 3$. (In Figure 1(a) there is a pass at $\bar{\nu}_1 = \bar{\nu}_2 = 1{\cdot}6$, but in the orthogonal direction.) The component due to the difference frequency potential is shown in Figure 3(b). This is, of course, identically zero along $\bar{\nu}_1 = \bar{\nu}_2$, and increases away from the diagonal. As a result, the total difference frequency QTF, shown in Figure 3(c), has a valley along the diagonal $\bar{\nu}_1 = \bar{\nu}_2$, with the lowest point near $\bar{\nu}_1 = \bar{\nu}_2 = 1{\cdot}5$.

Results for the sum frequency components in the case of $h/a = 1$ are shown in Figure 4 for the range $1 < \bar{\nu}_i < 2$. The quadratic force component in Figure 4(a) is similar to, though slightly lower in magnitude than, the corresponding result in Figure 1(a) for the longer cylinder. The sum frequency potential component in Figure 4(b) is substantially less than that for the longer cylinder, as is the total sum frequency force in Figure 4(c).

The influence of water depth is shown more clearly in Figure 5. Results are given for

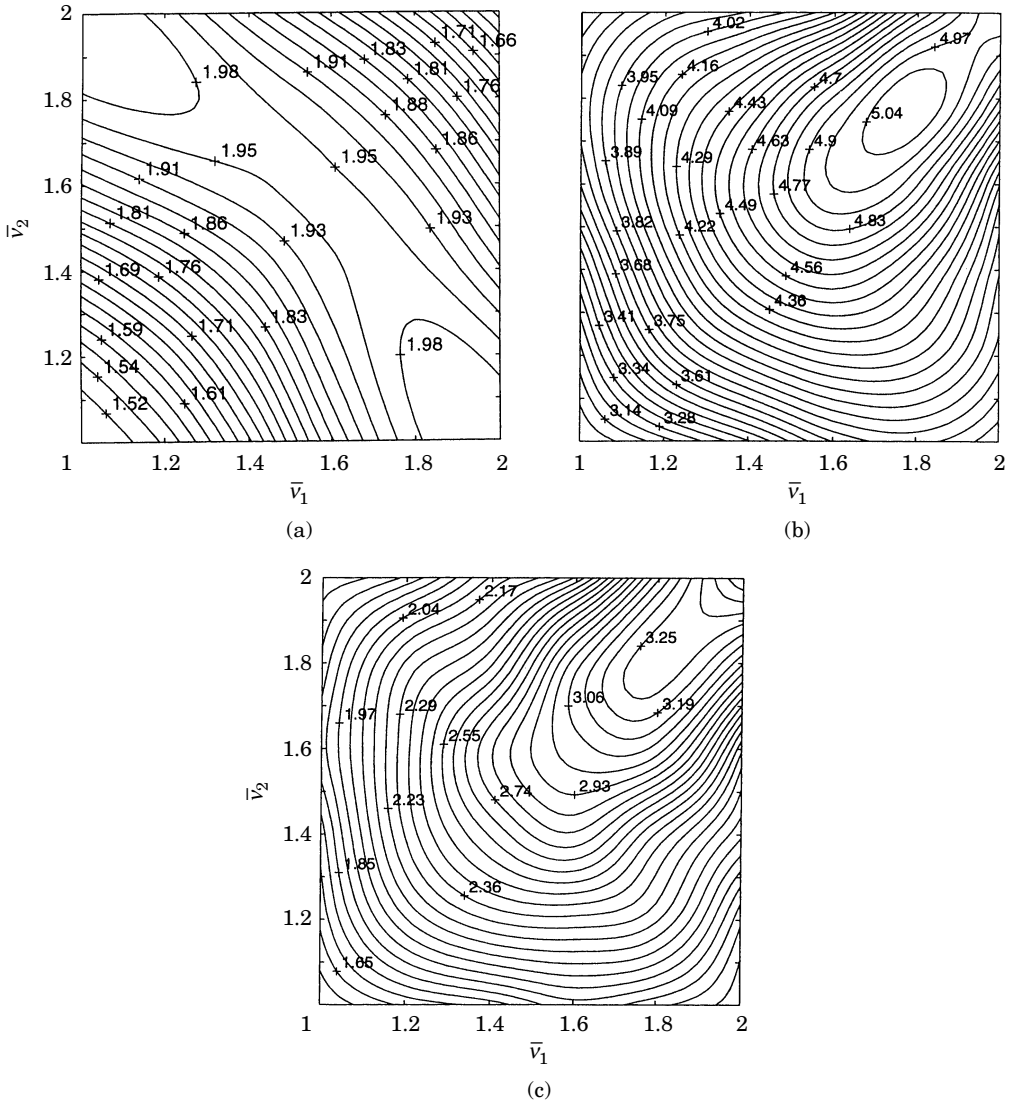

Figure 1. Contour plots of sum-frequency QTF ($1 < \bar{\nu}_i < 2$) for surge on a bottom-seated cylinder ($h/a = 4$): (a) quadratic term; (b) sum-frequency potential term; (c) total.

$h/a = 1$, 2, 4 and 10, based on the finite water depth theory; and results are also given for infinite water depth using the theory of Section 3.4 for the second-order particular solution. Figure 5(a) shows the quadratic force component, while Figure 5(b) shows the sum-frequency potential term, in both cases plotted against $\bar{\nu}_1$ for a constant difference frequency given by $\bar{\nu}_2 - \bar{\nu}_1 = 0{\cdot}2$. The quadratic terms in finite water depth are seen to converge to the infinite water depth case for increasing $\bar{\nu}_1$. This is not the case for the sum-frequency potential term: as discussed by Eatock Taylor & Hung (1987), this is because the second order sum-frequency potential has a more even distribution with depth than does the first-order potential. All the results, however, confirm that as the finite water depth solution is evaluated in increasing depths, the results converge to those for infinite depth.

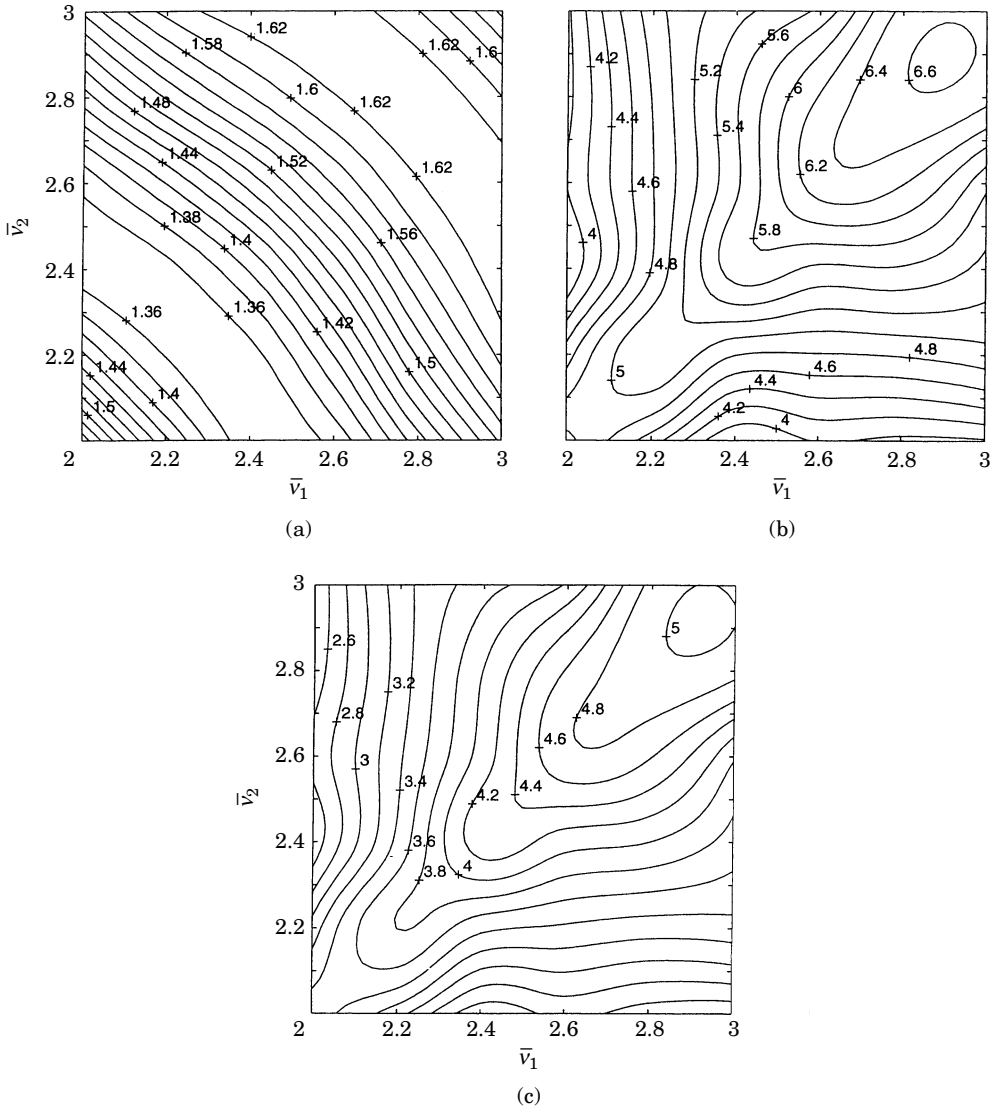

Figure 2. Contour plots of sum-frequency QTF ($2 < \bar{\nu}_i < 3$) for surge on a bottom-seated cylinder ($h/a = 4$): (a) quadratic term; (b) sum-frequency potential term; (c) total.

5.2. Free Surface Elevations

An important motivation for the analysis developed here is an interest in evaluating the diffracted wave field to second-order at any point in the free surface. This requires the direct solution we have developed for the second-order potential, rather than the indirect formulation which has been used by others to evaluate second-order forces. In this section we present some results in bichromatic waves for the case of the cylinder where $h/a = 4$. Although it is relatively straightforward to compute plots of the free surface using the method presented, it is not considered that an extensive set of such plots serves a useful purpose here. Rather, a sample of contour plots is given in Figures 6 and 7, and then consideration is given to the time history of wave run-up on the up-wave side of the cylinder, in each case for $\bar{\nu}_1 = 1{\cdot}2$, $\bar{\nu}_2 = 1{\cdot}8$.

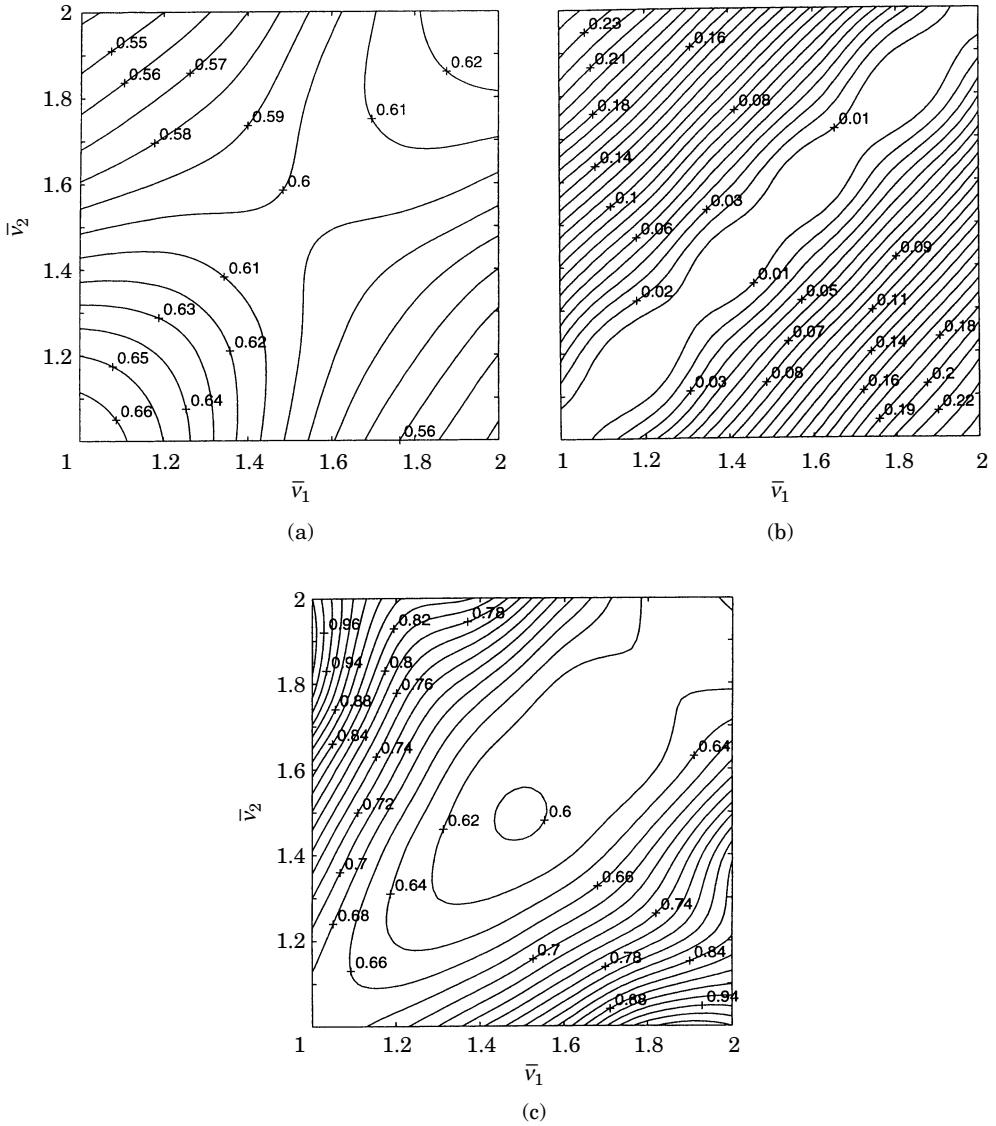

Figure 3. Contour plots of difference-frequency QTF ($1 < \bar{\nu}_i < 2$) for surge on a bottom-seated cylinder ($h/a = 4$): (a) quadratic term; (b) difference-frequency potential term; (c) total.

Figure 6(a) shows a contour plot of the maximum wave elevation over a square of side $10a$ centerd on the cylinder. The two waves have the same amplitude, $A_1 = A_2 = 0{\cdot}05a$, and have crests in phase at the axis of the cylinder. The maximum is given by the sum of first- and second-order wave contributions, and for different spatial positions this maximum occurs at different times. The contours correspond to the elevation divided by $(A_1 + A_2)$. Because the particular case shown in Figure 6(a) is for a rather small amplitude, the first-order contribution dominates. The contours of maximum defined in this manner are therefore very similar to the contours of first-order wave amplitude associated with the linear wave diffraction problem (for two incoming waves of the appropriate frequencies). If the effect of diffraction were

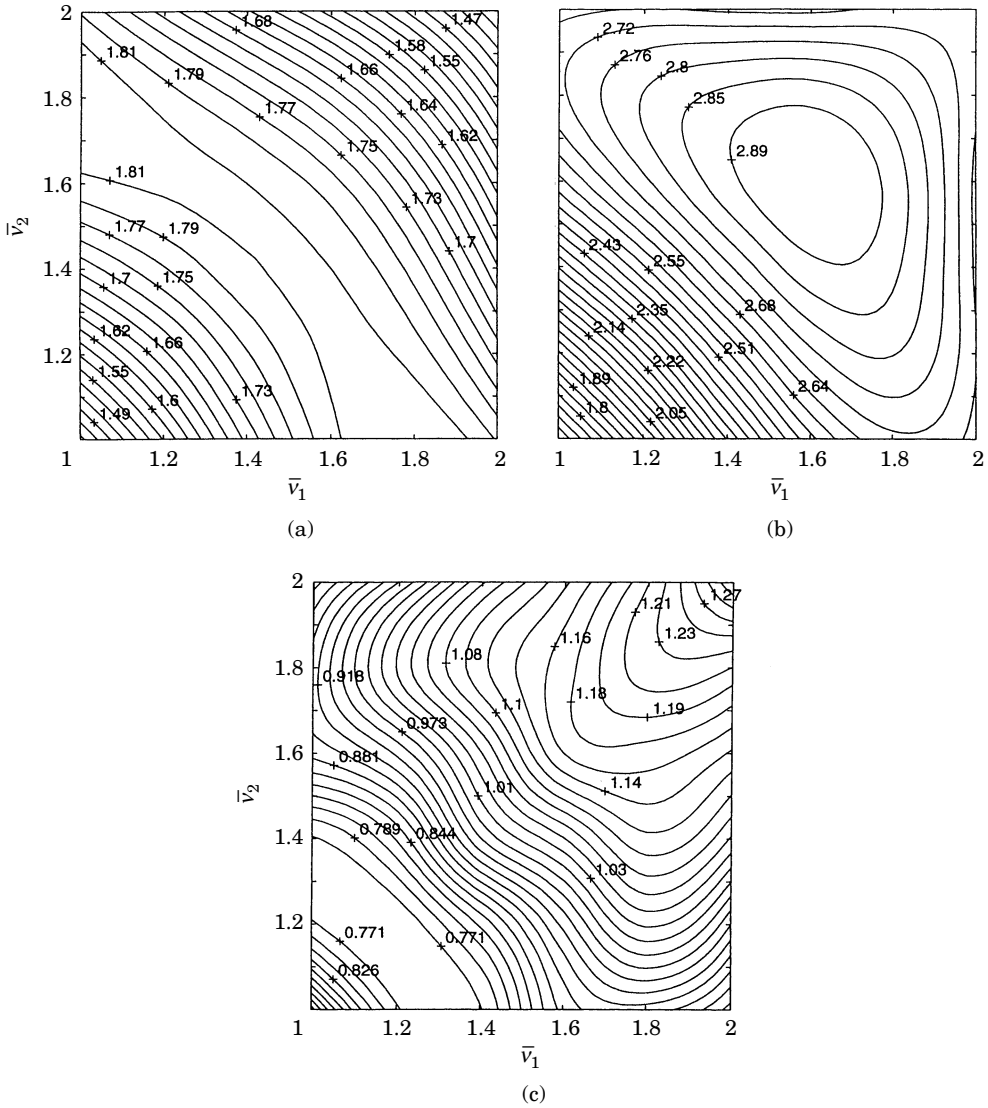

Figure 4. Contour plots of sum-frequency QTF ($1 < \bar{\nu}_i < 2$) for surge on a bottom-seated cylinder ($h/a = 1$): (a) quadratic term; (b) sum-frequency potential term; (c) total.

negligible (e.g. at much lower frequencies), the surface plotted would reduce to a horizontal plane of unit height.

Figure 6(b) shows analogous results, but for waves of higher amplitude, given by $A_1 = A_2 = 0{\cdot}25a$. Second-order effects are now more appreciable, and the maximum elevations are generally increased. The value on the up-wave face of the cylinder is well in excess of 2. The maximum in this latter quantity is found (numerically) to occur near the time $0{\cdot}16T$ after the crest of the incoming wave reaches $x = 0$ (for large y), where T is defined as $2\pi/(\omega_2 - \omega_1)$. Thus, T is the period of the second-order difference-frequency wave, which is twice the period of the low-frequency modulation of this wave pair. The behavior of the free surface in the general vicinity of the cylinder at $t/T = 0{\cdot}156$ is shown in Figure 7.

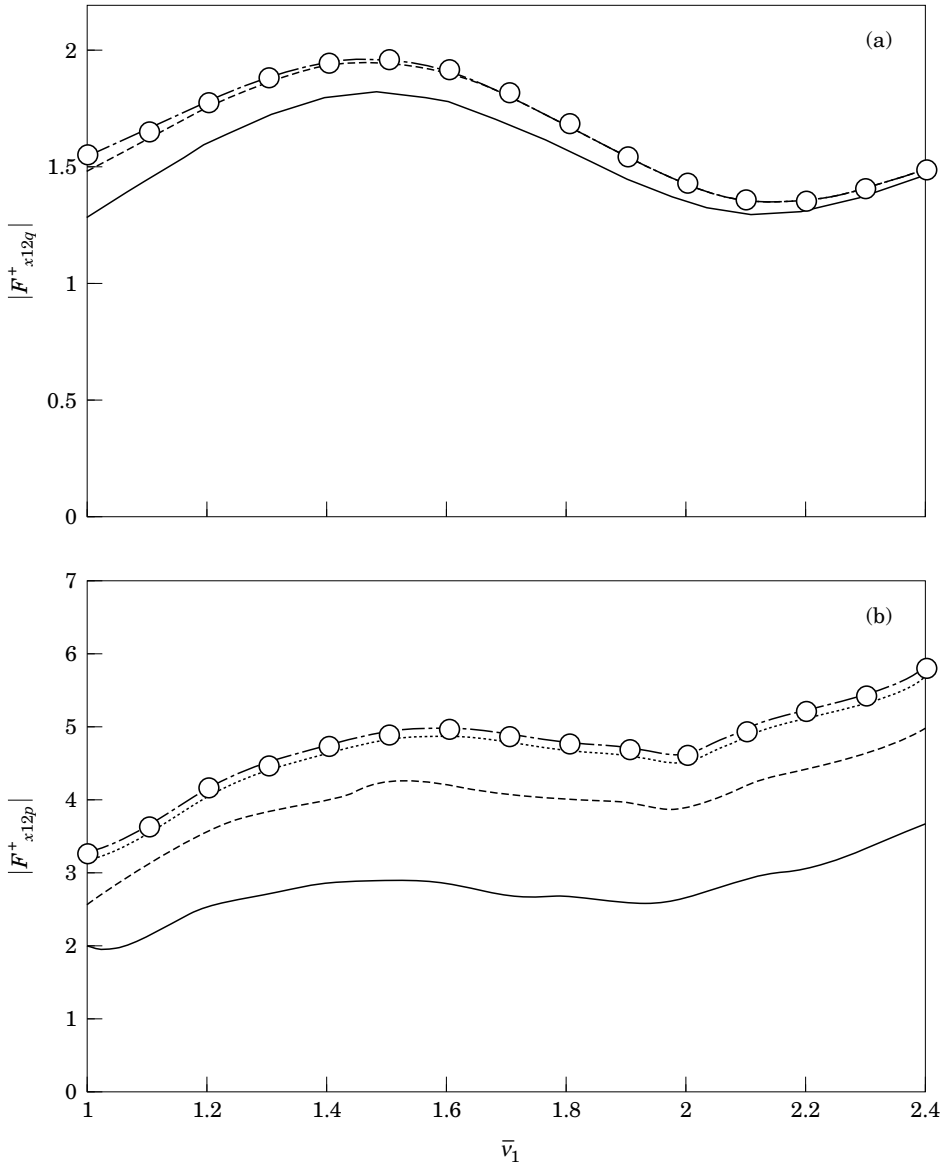

Figure 5. Influence of water depth on second-order surge force ($\bar{\nu}_2 - \bar{\nu}_1 = 0{\cdot}2$), for (a) quadratic component, and (b) sum-frequency potential component: (——), $h/a = 1$; (– – –), $h/a = 2$; (. . . . . .), $h/a = 4$; (– · – · –), $h/a = 10$; (○) $h/a = \infty$.

Figure 8 shows time histories of the wave elevation on the up-wave side of the cylinder (i.e. the wave run-up at $x/a = -1$, $y/a = 0$). Again this is for the case $\bar{\nu}_1 = 1{\cdot}2$, $\bar{\nu}_2 = 1{\cdot}8$, $A_1 = A_2 = 0{\cdot}25a$), and the two waves are in phase at the axis of the cylinder. The figure shows the behavior over the period T. The four lines correspond to: (a) the linear component, a modulated wave of period $2T$; (b) the second-order difference frequency wave, of period T; (c) the second-order sum frequency wave of period $2\pi/(\omega_1 + \omega_2)$; (d) the sum of the previous three components. Linear diffraction is seen to increase the local first-order wave elevation by around 70% above the incident wave, while the second-order component increases the first-order run-up by about 47% in

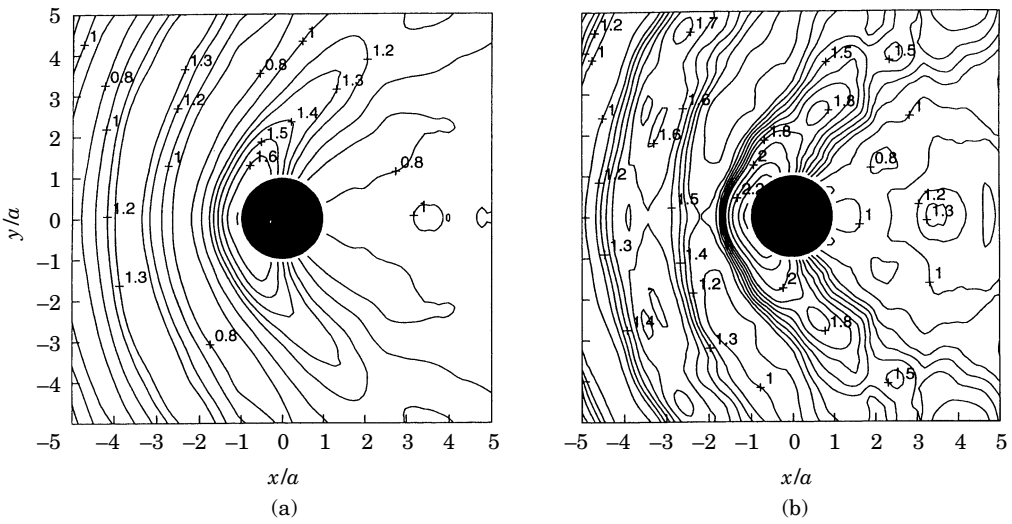

Figure 6. Contours of maximum free surface elevation (divided by $A_1 + A_2$) in the vicinity of the cylinder ($h/a = 4$): (a) $A_1/a = A_2/a = 0{\cdot}05$; (b) $A_1/a = A_2/a = 0{\cdot}25$.

this case. The effect of the second-order contribution is especially significant, because it has a maximum in phase with the maximum first-order run-up.

6. CONCLUSIONS

The semi-analytical solution for second-order diffraction of regular waves by a vertical cylinder has been extended to the case of a bichromatic incident wave field. Expressions have been obtained for sum- and difference-frequency potentials valid throughout the fluid domain. From these, we have obtained quadratic transfer functions for the sum- and difference-frequency forces on the cylinder, and these

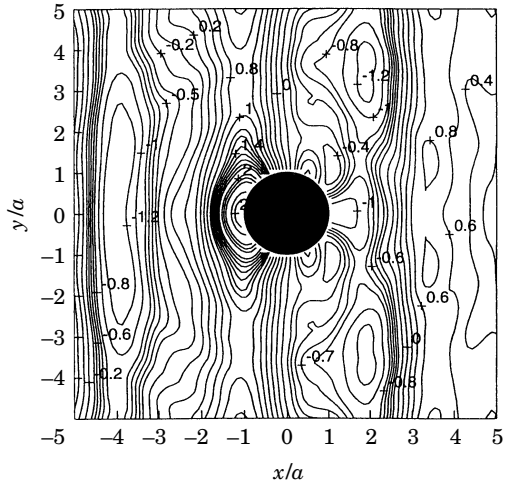

Figure 7. Contours of free surface elevation (divided by $A_1 + A_2$) in the vicinity of the cylinder ($h/a = 4$) at $t/T = 0{\cdot}1611$.

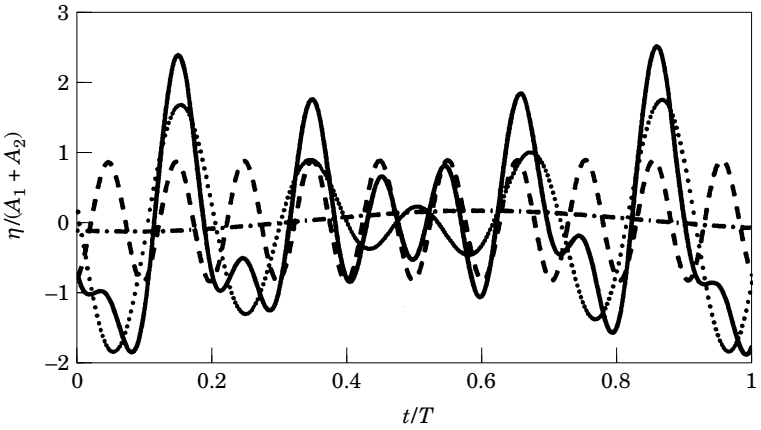

Figure 8. Time histories of run-up (divided by $A_1 + A_2$) at the up-wave face of the cylinder: (· · · · · ·), first-order component; (– · – · –), difference frequency component; (– – –), sum-frequency component; (——), total.

compare satisfactorily with results obtained at selected pairs of frequencies by Kim & Yue (1990) using a direct numerical scheme, and by Moubayed & Williams (1995) using an indirect approach. By using our semi-analytical method it is very easy to compute QTFs at a large number of frequency pairs, and we have therefore used contour plots to illustrate the frequency dependence of the second-order forces in bichromatic waves. The total sum-frequency surge force is found to have a ridge along the diagonal ($\omega_1 = \omega_2$), which tends to increase in height with increase in sum-frequency over the range considered. The total difference-frequency force, however, has a valley along the diagonal.

Our direct semi-analytical solution can also be used to obtain free surface elevations, and in particular to investigate the maximum run-up at a cylinder, as predicted by second-order theory. Our results have demonstrated that the maximum of the first- and second-order wave components of the run-up at the up-wave face of the cylinder can coincide, leading to a substantial local increase due to the second-order effects.

ACKNOWLEDGEMENTS

This work forms part of the research programme ''Uncertainties in Loads on Offshore Structures'' sponsored by EPSRC through MTD Ltd. (grant GR/J23167) and jointly funded with: Aker Engineering a.s., Amoco (UK) Exploration Company, BP Exploration Operating Co. Ltd., Brown & Root, Exxon Production Research Company, Health and Safety Executive, Shell UK Exploration and Production, Statoil, and Texaco Britain Ltd.

References

Abul-Azm, A. G. & Williams, A. N. 1988 Second-order diffraction loads on truncated cylinders. *ASCE Journal of Waterways, Port, Coastal and Ocean Division* **114,** 436–454.

Abul-Azm, A. G. & Williams, A. N. 1989a Approximation of second-order diffraction loads on arrays of vertical circular cylinders. *Journal of Fluids and Structures* **3,** 17–36.

Abul-Azm, A. G. & Williams, A. N. 1989b Second-order diffraction loads on arrays of semi-immersed circular cylinders. *Journal of Fluids and Structures* **3,** 365–388.

Chau, F. P. 1989 The second-order velocity potential for diffraction of waves by fixed offshore structures. Ph.D. Dissertation, University College London, University of London, U.K.

CHAU, F. P. & EATOCK TAYLOR, R. 1992 Second-order wave diffraction by a vertical cylinder. *Journal of Fluid Mechanics* **240,** 571–599.

CHEN, X. B., MOLIN, B. & PETITJEAN, F. 1991 Faster evaluation of resonant exciting loads on tension leg platforms. In *Offshore Engineering* **8,** 427–441. Plymouth: Pentech Press.

EATOCK TAYLOR, R. 1991 Assessment of springing in tension leg platforms. In *Advances in Marine Structures-2* (eds C. S. Smith & R. S. Dow), pp. 174–207. London: Elsevier Applied Science.

EATOCK TAYLOR, R. & HUNG, S. M. 1987 Second-order diffraction forces on a vertical cylinder in regular waves. *Applied Ocean Research* **9,** 19–30.

HERFJORD, K. & NIELSEN, F. G. 1986 Nonlinear wave forces on a fixed vertical cylinder due to the sum frequency waves in irregular seas. *Applied Ocean Research* **8,** 8–21.

GHALAYINI, S. A. & WILLIAMS, A. N. 1991 Nonlinear wave forces on vertical cylinder arrays. *Journal of Fluids and Structures* **5,** 1–32.

HUANG, J. B. & EATOCK TAYLOR, R. 1996 Semi-analytical solution for second-order wave-diffraction by a truncated circular cylinder in monochromatic waves. *Journal of Fluid Mechanics* **319,** 171–196.

KIM, M. H. & YUE, D. K. P. 1988 The non-linear sum frequency wave excitation and response of a tension leg platform. In *Proceedings of 5th International Conference on Behaviour of Offshore Structures, BOSS 88* (eds T. Moan, N. Janbu & O. Faltinsen), Vol. 2, pp. 687–703. Trondheim: Tapir Publishers.

KIM, M. H. & YUE, D. K. P. 1989 The complete second-order diffraction solution for an axisymmetric body. Part 1: monochromatic waves. *Journal of Fluid Mechanics* **200,** 235–264.

KIM, M. H. & YUE, D. K. P. 1990 The complete second-order diffraction solution for an axisymmetric body. Part 2: bichromatic incident waves and body motions. *Journal of Fluid Mechanics* **211,** 557–593.

KRIEBEL, D. L. 1992 Nonlinear wave interaction with a vertical circular cylinder. Part 2: wave run-up. *Ocean Engineering* **19,** 75–99.

LEE, C-H., NEWMAN, J. N., KIM, M.-H. & YUE, D. K. P. 1991 The computation of second-order wave loads. In *Proceedings of 10th International Conference on Offshore Mechanics and Arctic Engineering,* Vol. I-A, pp. 113–123. New York: ASME.

LIGHTHILL, M. J. 1979 Waves and hydrodynamic loading. In *Proceedings of 2nd International Conference on Behaviour of Offshore Structures, BOSS79* (eds H. S. Stephens & S. M. Knight), London, U.K., Vol. I, pp. 1–40. Cranfield: BHRA.

MCIVER, P. & EVANS, D. V. 1984 Approximation of wave forces on cylinder arrays. *Applied Ocean Research* **6,** 101–107.

MOLIN, B. 1979 Second-order diffraction loads on three-dimensional bodies. *Applied Ocean Research* **1,** 197–212.

MOUBAYED, W. I. & WILLIAMS, A. N. 1994 The second-order diffraction loads and associated motions of a freely floating cylindrical body in regular waves: an eigenfunction expansion approach. *Journal of Fluids and Structures* **8,** 417–451.

MOUBAYED, W. I. & WILLIAMS, A. N. 1995 Second-order hydrodynamic interactions in an array of vertical cylinders in bichromatic waves. *Journal of Fluids and Structures* **9,** 61–98.

NEWMAN, J. N. 1996 The second-order wave force on a vertical cylinder. *Journal of Fluid Mechanics* **320,** 417–443.